Eur. Phys. J. C (2024) 84:970
https://doi.org/10.1140/epjc/s10052-024-13302-7

THE EUROPEAN PHYSICAL JOURNAL C

Regular Article - Experimental Physics

Characterization of neutron-irradiated SiPMs down to liquid nitrogen temperature

Dania Consuegra Rodríguez[1,a] , **Rok Dolenec**[2,1,b] , **Peter Križan**[2,1,c] , **Samo Korpar**[3,1,d] , **Andrej Seljak**[1,e] , **Dejan Žontar**[1,f] , **Rok Pestotnik**[1,g]

[1] Experimental Particle Physics Department, Jožef Stefan Institute, Jamova cesta 39, 1000 Ljubljana, Slovenia
[2] Faculty of Mathematics and Physics, University of Ljubljana, Jadranska ulica 19, 1000 Ljubljana, Slovenia
[3] Faculty of Chemistry and Chemical Engineering, University of Maribor, Smetanova ulica 17, 2000 Maribor, Slovenia

Received: 12 April 2024 / Accepted: 27 August 2024 / Published online: 27 September 2024

Abstract Photodetectors used in future high-energy physics experiments will need to keep sufficient performance during a few years of data-taking despite radiation load, which, for example, in the planned upgrade of the Ring Imaging Cherenkov detectors in Large Hadron Collider beauty (LHCb) experiment is estimated at about 10^{13} 1-MeV neutron equivalent per cm^2 (neq/cm^2). Silicon photomultipliers (SiPMs) are considered as candidates for photodetectors for this application. However, their sensitivity to neutron irradiation may seriously compromise their operation, with the increase in dark count rates being the primary limitation after the irradiation. In this work, $1 \times 1\,\text{mm}^2$ 15 μm pitch NUV-HD-RH silicon photomultipliers developed by the Fondazione Bruno Kessler were characterized before and after the irradiation. In total, 5 SiPMs were irradiated at the Jožef Stefan Institute TRIGA nuclear reactor with different fluences from 10^9 neq/cm^2 up to 10^{13} neq/cm^2. The SiPMs were also annealed at high temperatures and re-characterized after the annealing. For the SiPM characterization in all the cases, current–voltage (I-V curve) measurements, dark count rate measurements, and waveform analysis, including single photon time resolution, were carried out at different controlled temperature steps from room temperature down to the liquid nitrogen temperature. While cooling to -20°C was enough for the SiPM irradiated at 10^9 neq/cm^2 to recover the ability to resolve single photons, by 10^{13} neq/cm^2, cooling to liquid nitrogen temperature was necessary. With sufficient cooling, the measured single photon time resolution was around 90 ps FWHM for all irradiation levels.

1 Introduction

The Large Hadron Collider beauty (LHCb) experiment at the European Organization for Nuclear Research (CERN) and the Belle II experiment at the High Energy Accelerator Research Organization (KEK) are two of the currently operational experiments in high energy physics searching for new phenomena beyond the Standard Model. For charged pion, kaon, and proton separation, both experiments rely on Ring Imaging Cherenkov (RICH) detectors [1,2]. In order to increase the size of the data sample of recorded events available for studies of rare processes, the next generation of experiments is under preparation with a much higher interaction rate. The LHCb experiment will be re-designed to operate at a luminosity of 1.5×10^{34} cm^{-2} s^{-1} [3], ten times that of the present detector. Due to the planned increased luminosity and, thus, higher background radiation, an upgrade of the RICH detectors is necessary. The increased background radiation to which the photodetectors will be exposed is one of the most challenging problems. They will have to keep sufficient performance during several years of data-taking despite radiation exposure, which is estimated at about 10^{13} 1-MeV neutron equivalent per cm^2 (neq/cm^2) [3]. One of the most promising candidates considered for the detection of Cherenkov photons is the silicon photomultiplier (SiPM). SiPMs are semiconductor photodetectors that have become a competitive choice in many fields [4–6], like nuclear medicine [7–9], high energy physics [10–13], and industrial and space applications [14–17]. Among their

[a] e-mail: dania.consuegra@ijs.si (corresponding author)
[b] e-mail: rok.dolenec@ijs.si
[c] e-mail: peter.krizan@ijs.si
[d] e-mail: samo.korpar@ijs.si
[e] e-mail: andrej.seljak@ijs.si
[f] e-mail: dejan.zontar@ijs.si
[g] e-mail: rok.pestotnik@ijs.si

benefits are high photon detection efficiency of up to 60% [18], high gain ($\sim 10^6$), and good timing resolution below 100 ps FWHM. In addition, they are small and robust photodetectors that do not require high operating voltages and can work in a magnetic field. All of these makes the SiPM a very promising photodetector for RICH applications [19], where the biggest drawback of the SiPMs is their susceptibility to radiation damage, with current devices not being able to withstand the background radiation levels expected in the upgraded RICH detectors of LHCb.

Analog SiPMs are composed of an array of single photon avalanche diodes (SPADs) connected in parallel, each reverse biased above breakdown voltage (V_{br}), thus, operating in Geiger-Müller mode [20]. However, thermal excitations can also trigger an avalanche, even when the SiPM is not exposed to light, leading to what is called the dark count rate (DCR). While the corresponding DCRs of current SiPMs are of the order of 10^5 Hz/mm^2 at room temperature [21], they can dramatically increase when the SiPM is exposed to radiation. Consequently, one of the main parameters affecting the operation of irradiated SiPMs is the increase in DCR [22,23]. One way to reduce the DCR is by cooling the SiPM as the DCR approximately halves every 10°C [6,18,24], although at some point saturation is reached [25,26].

In Si-based photodetectors, two types of damage are present due to radiation exposure: surface damage by ionizing energy loss (IEL) and bulk damage by non-ionizing energy loss (NIEL) [27]. For instance, neutron irradiation causes bulk damage by displacing atoms from their lattice site, thus creating crystal defects, e.g., Frenkel and cluster defects [28]. The degradation of neutron-irradiated SiPMs is mainly expressed as an increase in the leakage current (I_{leak}) and dark current (I_{dark}), i.e., the non-multiplied current and the current from the bulk that is multiplied in the Geiger–Müller mode, respectively. The DCR significantly increases proportionally to the irradiation fluence, leading to another important disadvantage: single photons can not be resolved anymore at room temperature when current SiPMs are irradiated beyond about 10^9 neq/cm^2 [29]. To some degree, SiPM operation after irradiation can be recovered through high-temperature annealing as reported in [30].

In this work, 1×1 mm^2 silicon photomultipliers developed by the Fondazione Bruno Kessler (FBK) were characterized before and after the irradiation. In total, 6 SiPMs were characterized before the irradiation, 5 of them were irradiated at the Jožef Stefan Institute (JSI) TRIGA nuclear reactor with fluences from 10^9 neq/cm^2 up to 10^{13} neq/cm^2, while leaving one of the SiPMs non-irradiated. One of the open questions is at which temperature the irradiated SiPMs could still be useful for RICH applications. Thus, the main objective of this contribution was to estimate the temperature at which single photons can be resolved after the irradiation. This paper is organized as follows. The experimental setup with details of the SiPM temperature stabilization are presented in Sect. 2. In Sect. 3, the obtained results for the current–voltage (I–V curve) measurements, the DCR measurements, and the waveform analysis, including single photon time resolution (SPTR), are shown before and after the irradiation at room temperature and at different controlled temperature steps down to the liquid nitrogen temperature. The results are discussed in Sect. 4, and finally, conclusions are given in Sect. 5.

2 Experimental setup

The SiPMs characterized were 1×1 mm^2 15 µm pitch FBK NUV-HD-RH UHD-DE SiPMs, based on the NUV-HD technology [31], and developed to improve the radiation hardness. For this purpose, the SiPMs were designed to have very small SPADs with fast recharge time (around 6 ns) to reduce saturation after the irradiation, even with high fluences. At the same time, the size of the non-active features of the SPAD was reduced to improve the fill factor and, thus, also the photon detection efficiency (around 40% at an overvoltage of 6 V and 420 nm). The SiPMs achieved a gain of approximately 9×10^5 at an overvoltage of 9 V, and the quenching resistance as reported by the producer is around 450 kOhm. Figure 1 shows an overview of the experimental setup for the SiPM characterization with details of the equipment used. More detailed descriptions of individual measurements are provided in the following sections. Common to all the measurements was the arrangement of the SiPM enclosure (Fig. 2): the SiPM and the custom electronics board were mounted inside a radio-frequency (RF) shielding box to minimize the electronic noise, which was necessary to enable good timing measurements.

The custom electronics board was composed of a SiPM RC bias filter and a high-speed NEC μPC2710TB pre-amplifier, based on an older RF gain block amplifier, with input impedance of 50 Ohm, power gain of 30 dB, and an upper limit operating frequency of 1.0 GHz [32]. In addition, the SiPM circuit bias loop was closed via an external KEITHLEY 6517B electrometer, holding a virtual ground for the SiPM. Hence, the *I–V* curve measurements, the DCR measurements, and the waveform analysis could be performed concurrently. Due to the overlapping design requirements necessary for cooling, laser illumination, and RF shielding, resulting in strict space constraints, as well as the necessity to measure different SiPMs with varying pin-outs, each characterized SiPM was connected to the custom electronics board through an approximately 5 cm long LEMO cable. Inside the RF shielding box, custom-made aluminum pieces ensured good thermal coupling between the RF shielding box and the SiPM, while 3D printed mechanical supports were used for optical isolation and alignment of

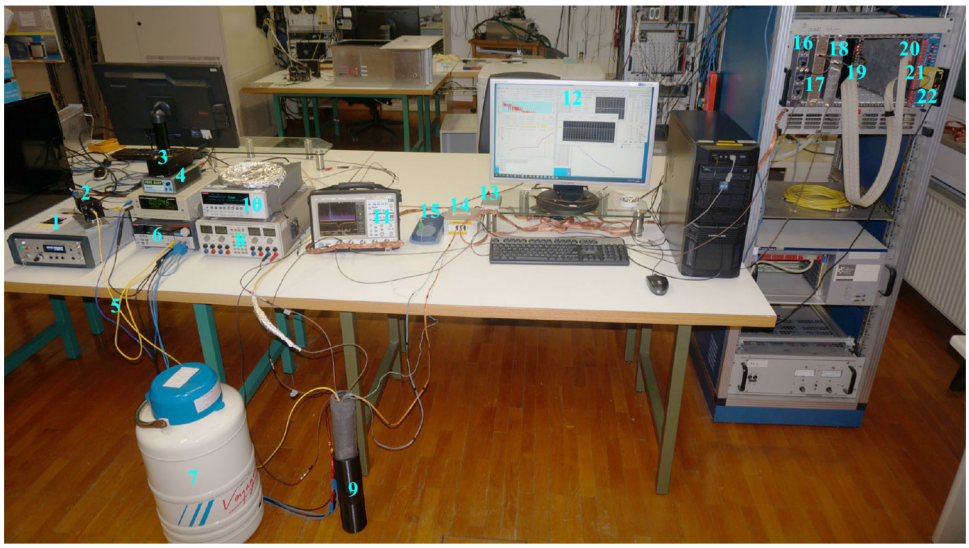

Fig. 1 Experimental setup: (1) ALPHALAS Picosecond Laser Diode Driver PLDD-20 M; (2) Laser shutter; (3) Laser shutter controller (Melles Girot electronic shutter controller); (4) GOPHER power supply for the laser shutter controller; (5) Optical fiber; (6) KEITHLEY power supply for the two resistive heaters; (7) Liquid nitrogen container; (8) HAMEG power supply for the pre-amplifier of the custom electronics board; (9) Cylindrical plastic container with a radio-frequency shielding box inside; (10) KEITHLEY 6517B electrometer; (11) LeCroy oscillosope; (12) National Instruments LabWindows data acquisition software; (13) DRS4 evaluation board; (14) Arduino temperature reader; (15) Picolog USB TC-08 thermocouple data logger; (16) Philips Quad rotary Attenuator Model 804; (17) ORTEC Octal Fast Timing Amplifier Model FTA820; (18) Octal divider; (19) Phillips Scientific 16 Channel discriminator latch CAMAC Model 7106; (20) CAEN 16 Ch ECL Scaler MOD C 257; (21) CAEN 16 Ch Universal Programmable I/O register MOD C 219; (22) LeCroy 8901A GPIB interface. Schematics of the setups used for individual measurements are shown in Figs. 3, 4, 5, 6

the SiPM. Light from an ALPHALAS 405 nm picosecond laser head, controlled by picosecond laser diode driver PLDD-20 M, was guided into the RF shielding box through a 2 m long optical fiber and was used to illuminate the SiPM at a single photon level. At the same time, three sensors were used to monitor the temperature and two resistive heaters were coupled to the external surface of the RF shielding box using thermal pads. Before starting each SiPM characterization, the RF shielding box was wrapped with thermal isolation (PE foam) and positioned in a cylindrical plastic container, which went inside the dry liquid nitrogen container. Dry liquid nitrogen containers are designed to absorb the liquid nitrogen in the walls and, in this way, keep the inside of the container at cryogenic temperatures without the need to submerge the experiment in liquid nitrogen itself. At the end of each SiPM characterization, the RF shielding box was removed from the cryogenic environment and thoroughly dried to prevent humidity condensation. All 6 SiPMs were operated at the same bias voltage (V_{bias}), calculated based on the producer specified V_{br} of 32.5 V and temperature coefficient of -25 mV/°C.

2.1 *I–V* curve measurements

For the *I–V* curve measurements (Fig. 3), a KEITHLEY 6517B electrometer provided the SiPM bias voltage between 0 V and 48 V in 0.1 V steps and measured the output current at each step by averaging 10 consecutive readings.

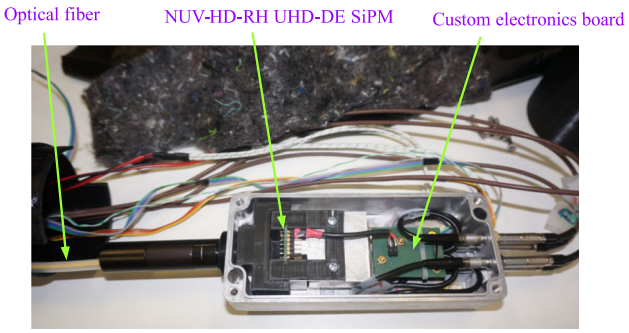

Fig. 2 Arrangement of the SiPM and the custom electronics board inside the radio-frequency shielding box

2.2 DCR measurements

For the DCR measurements (Fig. 4), the SiPM signal height threshold scans were performed at overvoltages between 3 V and 13 V in 2 V steps. First, the SiPM signal was pre-amplified using the custom electronics inside the RF shielding box, attenuated using Philips Quad rotary Attenuator Model 804, and additionally amplified using an ORTEC Octal Fast Timing Amplifier Model FTA820 to fit

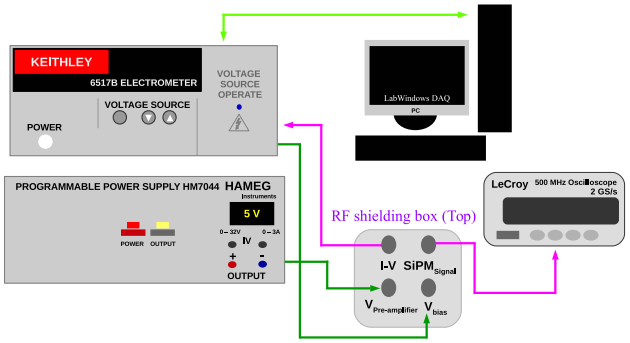

Fig. 3 Schematics of the setup used for the *I–V* curve measurements

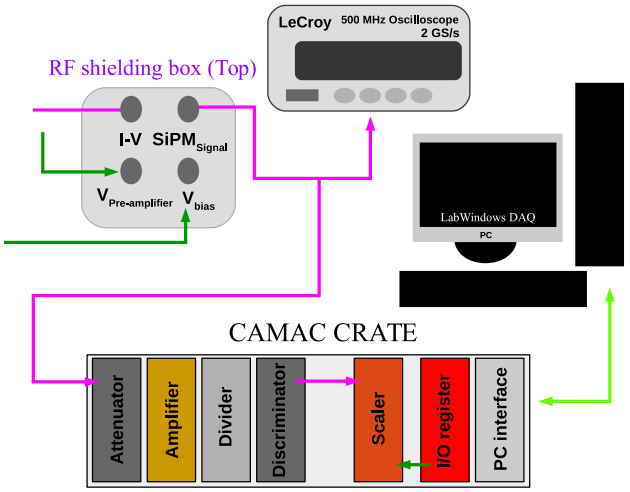

Fig. 4 Schematics of the setup used for the DCR measurements

the SiPM signal inside the digitizer dynamic range. Then, the signal was divided using a passive signal splitter with one half going to the discriminator (Phillips Scientific 16 Channel discriminator latch CAMAC Model 7106), where the threshold was computer controlled, increasing it 5 mV per step with 200 steps per threshold scan. The discriminator output pulse width was 110 ns, which limited the DCR measurement system dynamic range to a couple of MHz. At each step, the DCR was measured using a scaler (CAEN 16 Ch ECL Scaler MOD C 257) inside a 1 s long window controlled with the CAEN 16 Ch Universal Programmable I/O register MOD C 219.

2.3 Waveform analysis

For the waveform analysis (Fig. 5), the other half of the divided signal was digitized at 5 GS/s using Paul Scherrer Institute (PSI) DRS4 Domino Ring Sampler evaluation board [33] with 10^6 waveforms collected per measurement. In front of the optical fiber, a computer-controlled shutter blocked the laser light during all measurements except for the waveform

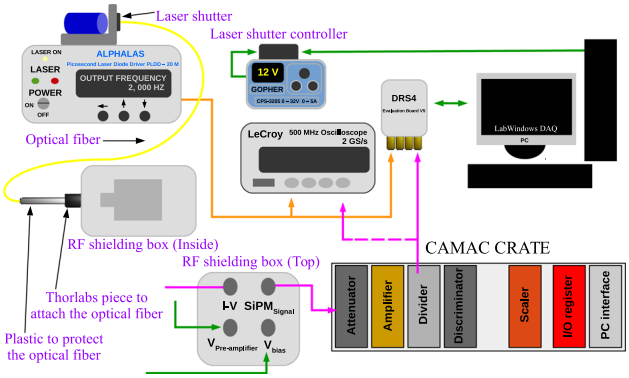

Fig. 5 Schematics of the setup used for the waveform analysis

acquisitions. The post-processing of the data was performed using the ROOT analysis framework [34].

A challenging aspect of good timing measurements was the electronic noise. Although it was suppressed mainly by the RF shielding box, inside which the SiPM and the custom electronics board with its pre-amplifier were enclosed, long cables between the pre-amplifier and the modular electronics necessary to place the SiPMs inside the dry liquid nitrogen container, as well as additional circuitry and cabling needed for the I-V curve measurements, led to some remaining noise visible as an additional contribution in the timing distributions.

2.4 Temperature stabilization

Figure 6 (top) shows the schematics of the setup for temperature stabilization. An effort was made to optimize the total measurement time, which still ended at $\sim$ 14 h per SiPM characterization. Some steps had to be done manually, like changing the SiPMs and placing the setup inside the dry liquid nitrogen container. However, after that, the measurement protocol was performed automatically using custom National Instruments LabWindows data acquisition (DAQ) software. The most time-consuming was that measurements had to be carried out at multiple temperatures. First, a temperature stabilization was needed, and then, the measurements at each stabilized temperature step took approximately 1 h 20 min. Thus, measurements were only carried out at room temperature ($\sim$ 23°C), $-$ 20°C, $-$ 60°C, $-$ 100°C, $-$ 140°C, and liquid nitrogen temperature. More exactly, in this work, the lowest measurement temperature was not $-$ 196°C but approximately $-$ 187°C because this is where the equilibrium was reached between the liquid nitrogen cooling and the heating of the setup.

The RF shielding box was heated to the targeted temperature by two resistive heaters thermally coupled to the external surface of the RF shielding box, while three sensors were used to monitor the temperature (Fig. 6, bottom). One of

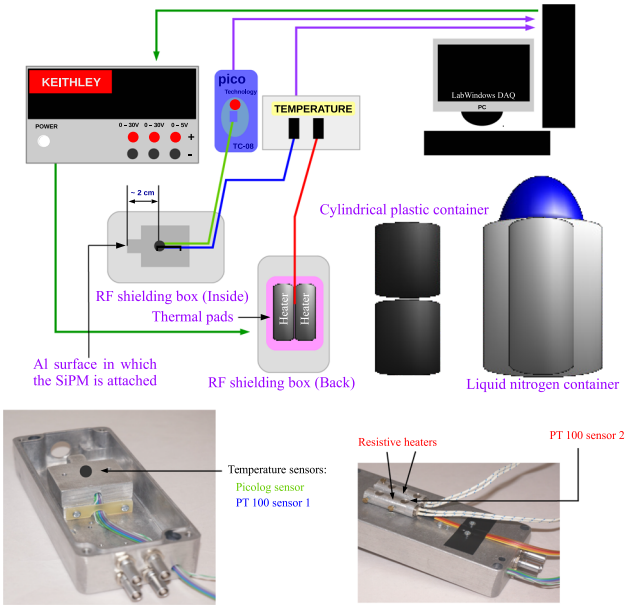

Fig. 6 Schematics of the setup used for temperature stabilization (top); customizing the radio-frequency shielding box (bottom)

the sensors (a PT 100 sensor) was placed between the resistive heaters and the RF shielding box. The other two sensors (another PT 100 sensor and a Picolog K-type sensor) were inserted inside the aluminum block at ~ 2 cm distance from the SiPM. The Picolog sensor was used to calibrate the PT 100 sensor placed close to the SiPM, and the temperatures from the two PT 100 sensors were readout using Arduino-based electronics. Based on these temperature readouts, the voltage applied to the two resistive heaters was adjusted using custom DAQ software to reach and stabilize the targeted temperature. A separate calibration measurement was performed to determine the correlation between heating power (heater voltage) and SiPM temperatures, and additionally, the voltages were adjusted in real-time proportionally to the square of temperature deviation (Eq. (1)).

$$V_a(t) = V_c(T_s) - sgn(T_m(t) - T_s) \times k \times (T_m(t) - T_s)^2, \quad (1)$$

where $V_a(t)$ is the total real-time voltage applied to the heaters, $T_m(t)$ is the real-time temperature measured with the PT 100 sensor 1, T_s is the temperature set as a target, and k is a constant (set to a value of about 2). Based on the previously mentioned separate calibration, $V_c(T_s)$ is the expected total voltage to be applied to the heaters for the temperature set as a target. This procedure enabled reaching target temperatures within $\pm$ 2°C, except at room temperature where the temperature was stabilized at $\sim$ 23°C and at liquid nitrogen temperature where equilibrium at approximately $-$ 187°C was reached as explained above. During all measurements, the stability of the reached temperature was maintained with

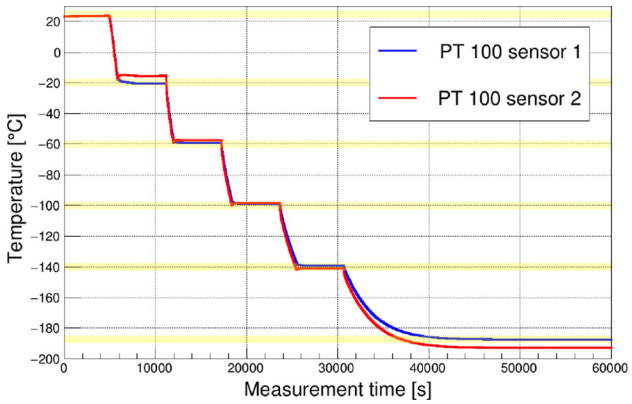

Fig. 7 Temperature stabilization as recorded by the PT 100 sensors

fluctuations of less than 1°C (Fig. 7). The slight difference in behavior of the two PT 100 sensors is due to their position: at high temperatures, sensor 2 readings are above sensor 1 readings due to the heating of the resistive heaters, while at low temperatures, sensor 2 readings are lower than sensor 1 readings because sensor 2 was more exposed to the cryogenic environment.

2.5 Irradiation and annealing of the SiPMs

After characterizing each SiPM before the irradiation, 5 SiPMs were irradiated inside the triangular channel of the 250 kW TRIGA nuclear reactor of the JSI [35]. The SiPMs were exposed to 5 different fluences: 10^9 neq/cm^2, 10^{10} neq/cm^2, 10^{11} neq/cm^2, 10^{12} neq/cm^2, and 10^{13} neq/cm^2. No V_{bias} was applied to the SiPMs during the irradiation. The irradiation time per SiPM was 143 s, with reactor power adjusted to reach each targeted fluence. The irradiation was performed at room temperature, and the whole process took approximately 15 min; thus, the annealing during the irradiation can be neglected. The SiPMs were kept inside a freezer at $-$ 25°C all the time in between the irradiation and the re-characterization after the irradiation. The temperature of annealing was set to 80°C according to producer recommendation except for the SiPM irradiated at 10^9 neq/cm^2 where the annealing at 110°C was explored.

3 Results

3.1 *I–V* curve measurements

Before the irradiation, the 6 SiPMs showed very similar behavior at room temperature (Fig. 8, top-left): the current had a very gentle dependence on V_{bias} until the V_{br} and after the V_{br} it exponentially increased until overvoltage (the voltage in excess of V_{br}) of about 10 V, where

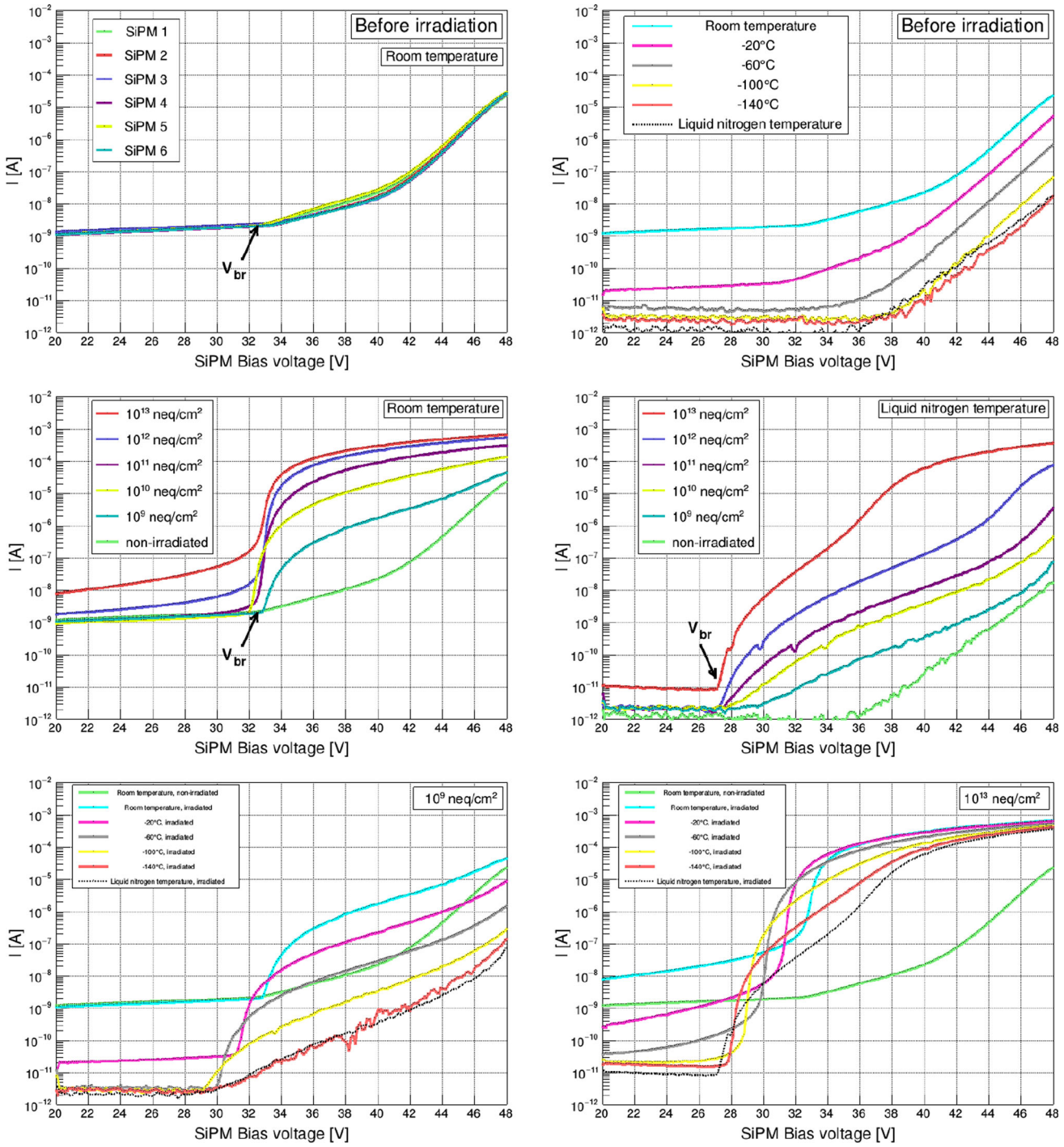

Fig. 8 *I–V* curve measurements for: each of the SiPMs at room temperature before the irradiation (top-left); one of the SiPMs at different temperatures before the irradiation (top-right); each of the SiPMs at room temperature after the irradiation (middle-left); each of the SiPMs at liquid nitrogen temperature after the irradiation (middle-right); the SiPM irradiated at 10^9 neq/cm^2 at different temperatures (bottom-left); the SiPM irradiated at 10^{13} neq/cm^2 at different temperatures (bottom-right)

correlated noise started to prevail. As expected, the current decreased, and the V_{br} slowly shifted to lower values when a SiPM was cooled down (Fig. 8, top-right), where it has to be noted that the smallest measurable current was limited by the electrometer accuracy (about 3 pA), as seen for temperatures below − 20°C. After the irradiation, the *I–V* curve measurements clearly showed the neutron damage effects: at room temperature the current significantly increased between irradiation fluences (Fig. 8, middle-left), and this behavior remained seen at liquid nitrogen temperature (Fig. 8, middle-right). The V_{br} seems unaffected by irradiation (black arrows in Fig. 8). The I–V curve measurements at different temperatures for two specific fluences were compared to the I–V curve measurement of the non-irradiated SiPM at room temperature. For example, at 10^9 neq/cm^2 the current matched the non-irradiated measurement at approximately − 60°C around useful overvoltage (Fig. 8, bottom-left). In contrast, at 10^{13} neq/cm^2, even at liquid nitrogen temperature, the current did not decrease to the original level at useful overvoltage (Fig. 8, bottom-right).

3.2 DCR measurements

Before the irradiation, the DCR behaved as expected: it increased with overvoltage (Fig. 9) until reaching the limits of the system dynamic range at an overvoltage of ∼ 13 V and decreased with temperature by a factor of 2.2 per 10°C (Fig. 10, top-right), whereby at − 100°C only the electronics noise remained. Also, before the irradiation, the DCR measured with the 6 SiPMs showed good agreement at room temperature and an overvoltage of 9 V (Fig. 10, top-left). After the irradiation, all of the SiPMs are at or close to the maximum of the system dynamic range at room temperature and an overvoltage of 9 V (Fig. 10, middle-left), and the steps in the threshold scan representing different numbers of SPADs triggered quickly get lost. Cooling, of course, helps (Fig. 10, bottom-left). However, for the SiPM irradiated at 10^{13} neq/cm^2, the steps can not be seen at all, even at the liquid nitrogen temperature (Fig. 10, middle-right). The DCR measurements at different temperatures for specific fluences were compared to the DCR measurement of the non-irradiated SiPM at room temperature. For example, the DCR of the SiPM irradiated at 10^9 neq/cm^2 was comparable to the DCR of the non-irradiated SiPM close to − 60°C (Fig. 10, bottom-left). In contrast, at 10^{13} neq/cm^2 the DCR never matched the original level, and was close to the maximum of the system dynamic range at most temperatures. At 10^{12} neq/cm^2, the DCR at original level could be reached somewhere between −140°C and liquid nitrogen temperature (Fig. 10, bottom-right).

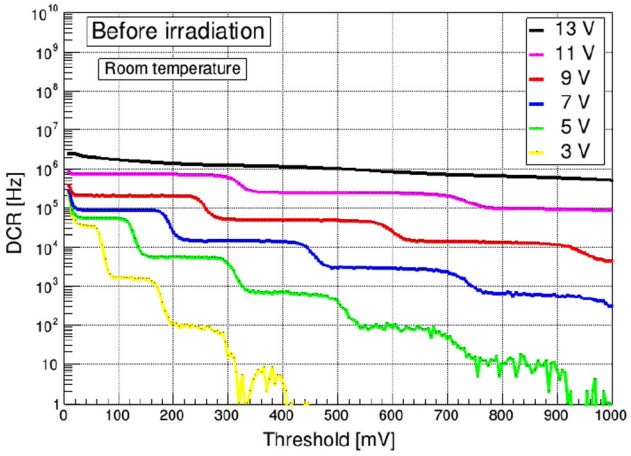

Fig. 9 DCR measurements for one of the SiPMs at room temperature before the irradiation for different overvoltages

3.3 Waveform analysis

On the oscilloscope, signals from single SPADs could be seen (Fig. 11, top). From the waveforms, many quantities could be measured, for example, the pulse height, the charge (Fig. 11, bottom-left) as well as the timing (Fig. 11, bottom-right). The charge was obtained by integrating the waveforms inside a 60 ns gate around the signal peak. The timing was calculated as the difference between the linearly interpolated 40% maximum amplitude crossing time of the waveforms belonging to the laser and the SiPM. To obtain the SPTR, a single photon cut (SP-cut) was always performed on the charge (red area in Fig. 11, bottom-left) within ± 1σ interval determined from the Gaussian fit of the single photon peak. The SPTR values reported were obtained from a triple Gaussian fit over the timing distributions with the FWHM calculated from the fit function.

Before the irradiation, the SPTR values were around 90 ps FWHM independent of the temperature. After the irradiation, the single photons could not be resolved anymore at room temperature and an overvoltage of 9 V, even for the SiPM irradiated at 10^9 neq/cm^2. It has also been observed that the noise contribution moved relative to the main peak of the timing distributions with changing temperatures (blue arrows in Fig. 12). This could possibly be explained by the temperature dependence of the electrical properties of the pre-amplifier and/or of the other components of the custom electronics board and even of the long cables. Besides, the SiPM operation at cryogenic temperatures is not straightforward due to the temperature dependence of its electrical properties. For example, in [36], it was observed that between 300 K (27°C) to 77 K (− 196°C), the quenching resistance and, thus, the recharge time of the SPAD, increases by a factor of 10, while the junction capacitance decreases by less than a factor of 2.

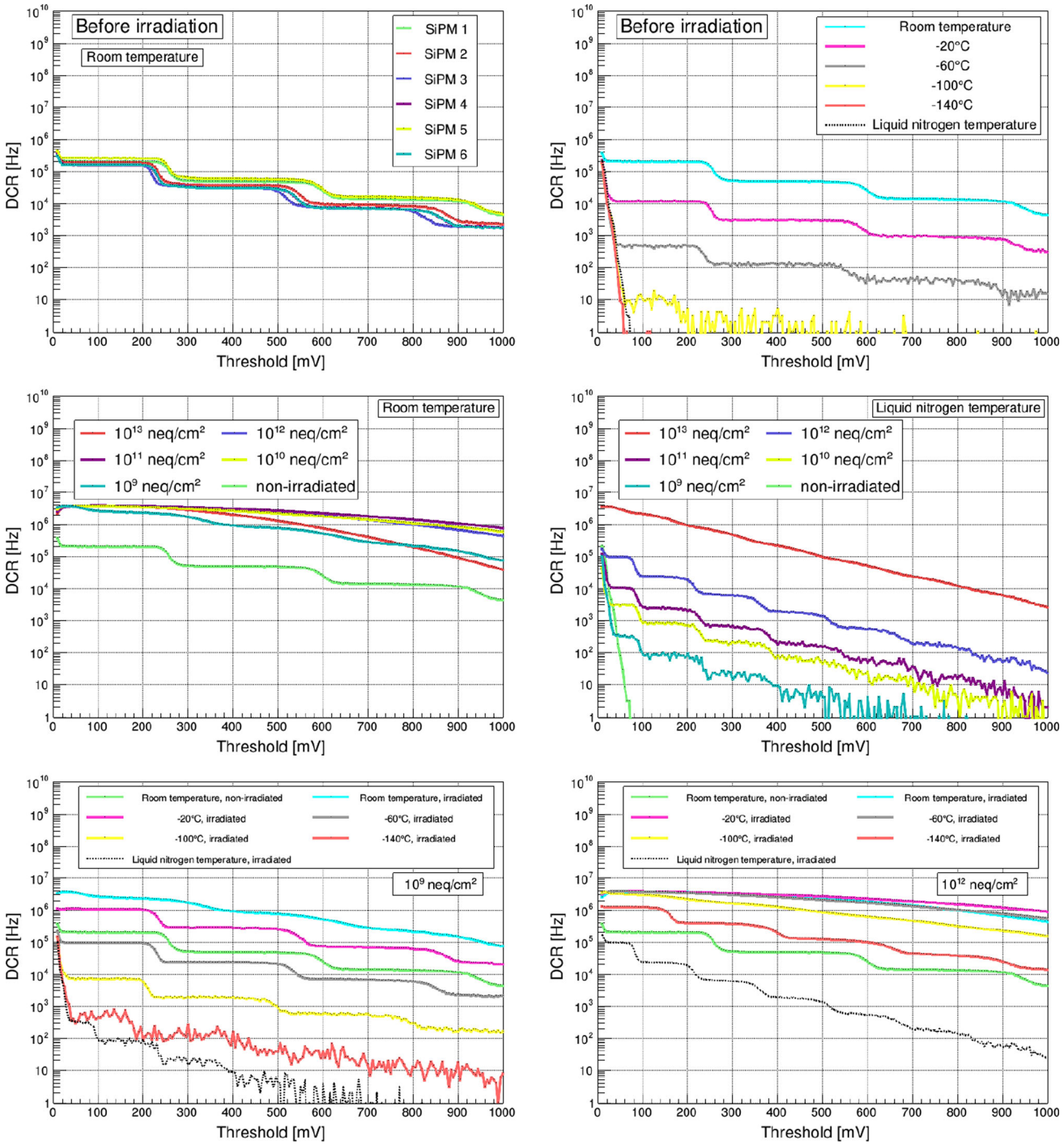

Fig. 10 DCR measurements for: each of the SiPMs at room temperature and an overvoltage of 9 V before the irradiation (top-left); one of the SiPMs at different temperatures before the irradiation (top-right); each of the SiPMs at room temperature after the irradiation (middle-left); each of the SiPMs at liquid nitrogen temperature after the irradiation (middle-right); the SiPM irradiated at 10^9 neq/cm^2 at different temperatures (bottom-left); the SiPM irradiated at 10^{12} neq/cm^2 at different temperatures (bottom-right)

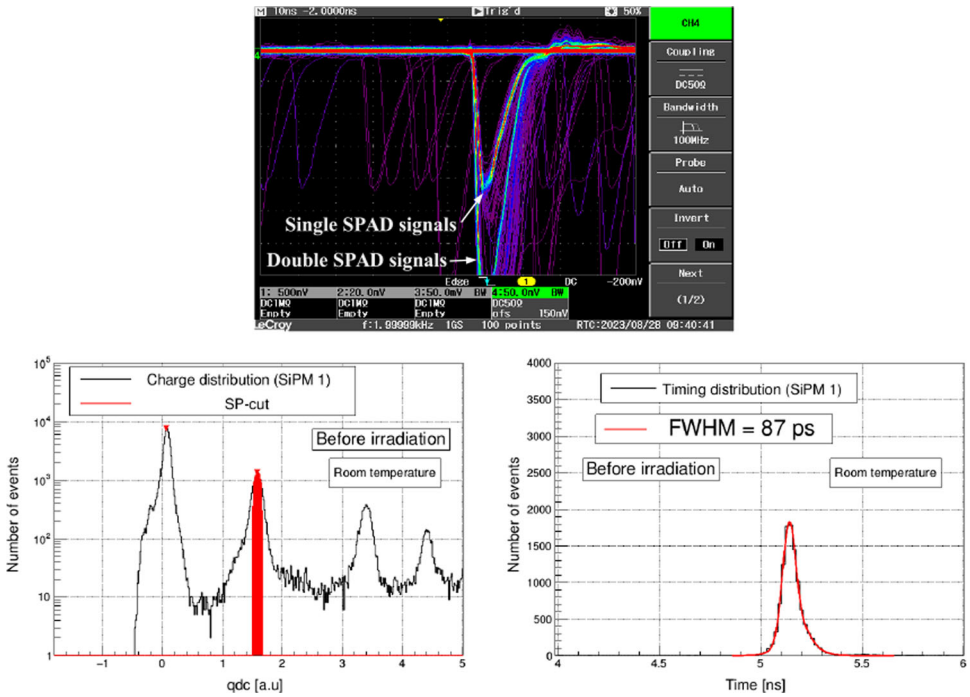

Fig. 11 Before the irradiation: SiPM signal shape at room temperature and an overvoltage of 9 V (top); charge distribution at room temperature and an overvoltage of 9 V with single photon cut shown in red (bottom-left); timing distribution at room temperature and an overvoltage of 9 V with the SPTR expressed in FWHM (bottom-right)

The metric used in this work to determine the temperature, at which irradiated SiPMs can still be useful for RICH application, was defined as the temperature at which single photons can be resolved in the charge distributions at an overvoltage of 9 V. For example, Fig. 12 (left) shows the charge distributions at an overvoltage of 9 V of the SiPM irradiated at 10^{12} neq/cm^2, from which it can be seen that single photons can not be resolved at higher temperatures. For this irradiation level, − 140°C was selected as the temperature of stable operation, as the single photon peak became again clearly visible. The choice of metric was supported by the timing distributions, where it can also be seen that a good SPTR is reestablished at around − 140°C (Fig. 12, right). The temperatures of stable operation at different fluences, as estimated by this definition, are shown in Fig. 13. At 10^{13} neq/cm^2, cooling to liquid nitrogen temperature is necessary while − 20°C seems enough for SiPM irradiated at 10^9 neq/cm^2. At the so-defined temperatures, the SPTR after the irradiation is shown for each fluence in Fig. 14. The SPTR does not seem to be affected by irradiation as long as single photons can be resolved. However, there are still small fluctuations due to the remaining background contribution, as indicated by the best SPTRs obtained for the irradiated SiPMs at any overvoltage or temperature (green line in Fig. 14). Only at 10^{13} neq/cm^2, SPTR below 100 ps FWHM could not be recovered, as cooling to liquid nitrogen temperature was barely sufficient for this irradiation level.

3.4 Annealing of the SiPMs

All the SiPMs were annealed at 80°C for 24 h except the SiPM irradiated at 10^9 neq/cm^2 for which the annealing results reported are after a total annealing of 3 months at room temperature and additional annealing at 110°C for 24 h. For all the irradiated SiPMs, after the annealing, a slight decrease in the current was observed (Fig. 15, top), which is more pronounced in the I_{leak} for the SiPM irradiated at 10^{13} neq/cm^2 and in the I_{dark} for the SiPMs irradiated at lower fluences ($< 10^{12}$ neq/cm^2). After the annealing, a decrease in the DCR was also observed for all the irradiated SiPMs (Fig. 15, bottom), although the improvement is minor for the SiPM irradiated at 10^{13} neq/cm^2. In contrast, for the SiPM irradiated at 10^9 neq/cm^2, the DCR at liquid nitrogen temperature reaches levels below the electronics noise.

Annealing at the conditions used in this work did not improve operational temperatures where single photons could be resolved at an overvoltage of 9 V (Fig. 13). While the improvement could be sufficient to enable operation at slightly higher temperatures, the temperature increase could not be resolved by the 40°C steps where measurements were carried out in this work. The SPTR does not seem to be affected by annealing as long as single photons can be resolved. Though the background contribution remains, for the SiPM irradiated at 10^{13} neq/cm^2 after the annealing, SPTR values lower than 100 ps FWHM were measured at liquid nitrogen temperature and overvoltages of 5 V and 7 V.

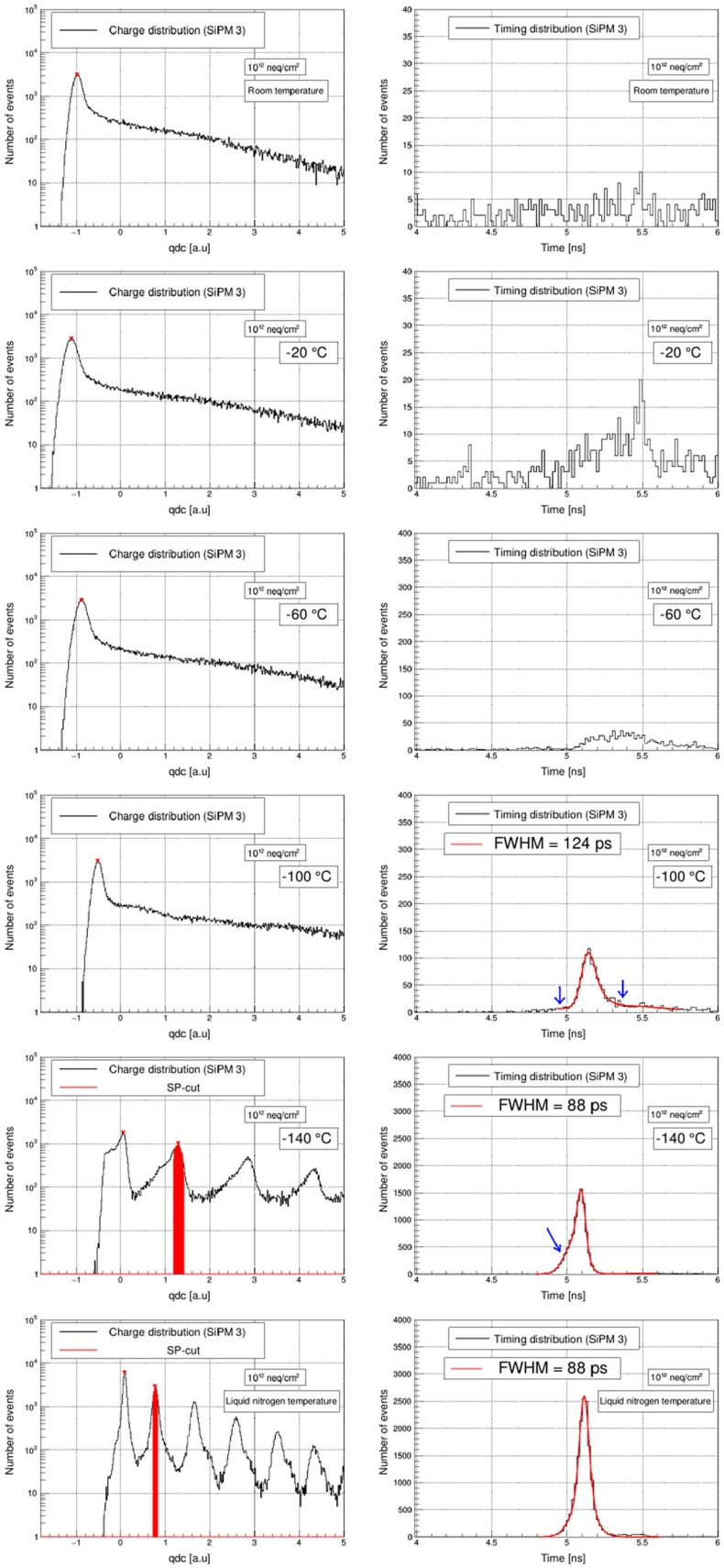

Fig. 12 For the SiPM irradiated at 10^{12} neq/cm^2 at different temperatures: charge distributions at an overvoltage of 9 V with SP-cut included when possible (left); timing distributions at an overvoltage of 9 V with the SPTR expressed in FWHM (right). Arrows indicate how the noise contribution moved relative to the main peak as discussed in sub-section 3.3

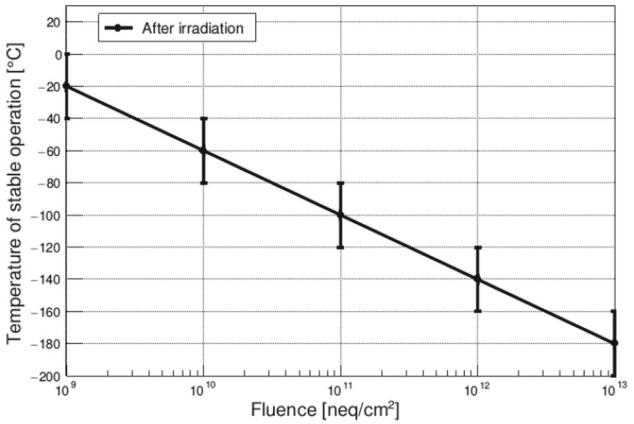

Fig. 13 The temperatures at which single photon can be resolved at an overvoltage of 9 V vs. different irradiation levels. The error bars indicate the 40°C steps in which the measurements were carried out in this work

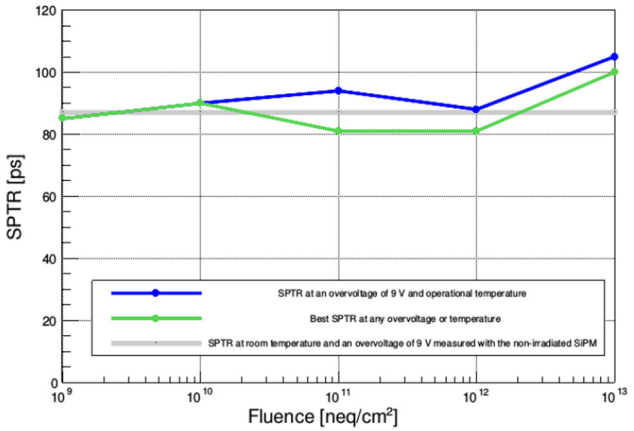

Fig. 14 The SPTR at an overvoltage of 9 V and operational temperatures as defined in Fig. 13 vs. different irradiation levels with the SPTR at room temperature and an overvoltage of 9 V measured with the non-irradiated SiPM shown in gray

4 Discussion

Considering the specific requirements of the planned RICH detector upgrades, to achieve a timing resolution below 100 ps FWHM, the DCR needs to be low enough so that single photons can still be resolved and single photon cut can be applied to the data, all at high SiPM overvoltage necessary for good timing. By this definition, cooling to − 140 °C and − 180 °C was necessary after the irradiation at 10^{12} neq/cm^2 and 10^{13} neq/cm^2, respectively (Fig. 13). Another, although more strict, requirement could be that the DCR at single photon level, after the irradiation but with cooling, should be on the same level as before the irradiation at room temperature and an overvoltage of 9 V. In Fig. 16, the DCRs for different irradiation levels and temperatures are plotted and compared to the DCR before the irradiation at room temperature and an overvoltage of 9 V (gray line). It can

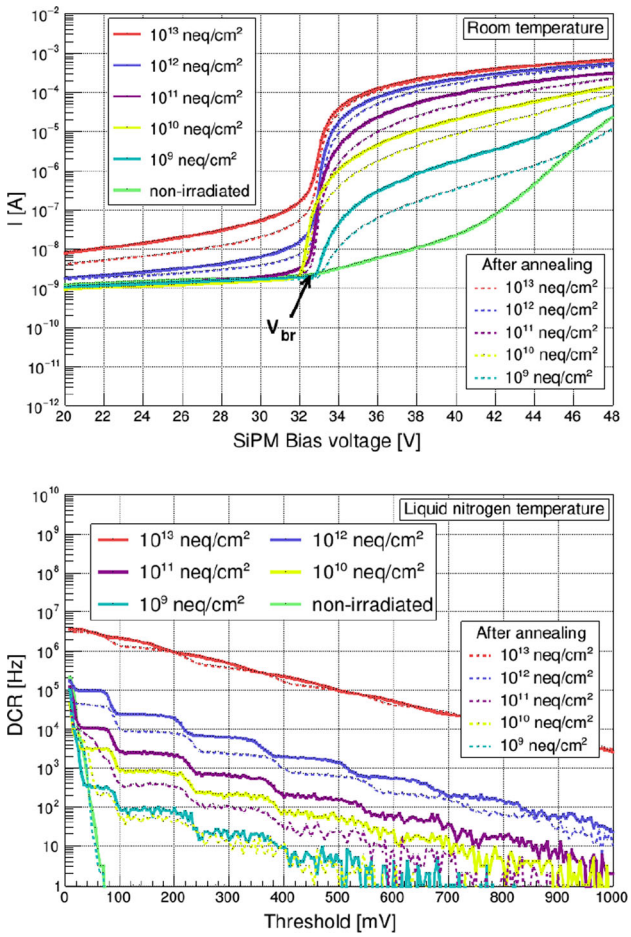

Fig. 15 *I–V* curve measurements for each of the SiPMs at room temperature before and after the annealing (top); DCR measurements for each of the SiPMs at liquid nitrogen temperature before and after the annealing (bottom). Dashed lines were used to plot data after the annealing

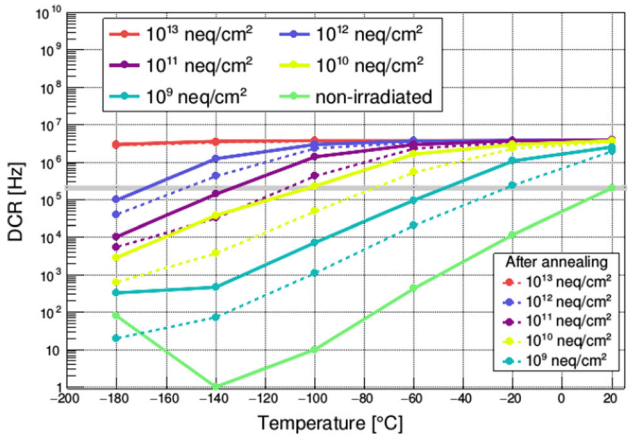

Fig. 16 DCR vs. temperature before and after the annealing at different fluences and an overvoltage of 9 V. Dashed lines were used to plot data after the annealing while the gray line indicates the DCR at room temperature and an overvoltage of 9 V measured with the non-irradiated SiPM

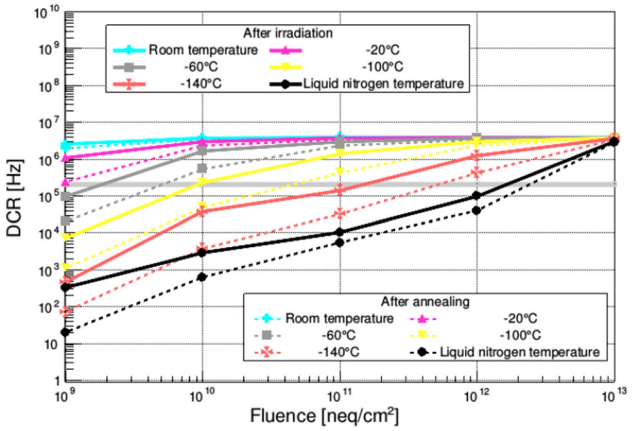

Fig. 17 DCR vs. fluence at different temperatures before and after the annealing and an overvoltage of 9 V. Dashed lines were used to plot data after the annealing, while the gray line indicates the DCR at room temperature and an overvoltage of 9 V measured with the non-irradiated SiPM

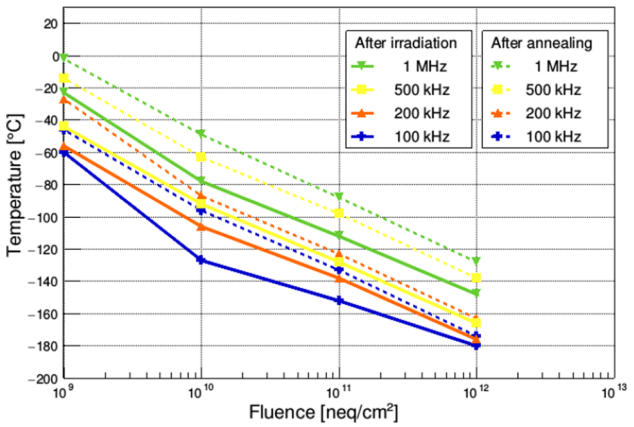

Fig. 18 Temperature required to reach different DCR levels at different fluences. Dashed lines were used to plot data after the annealing. At fluence of 10^{13} neq/cm^2, the DCR never reaches the levels included in this plot (Fig. 16)

be seen that the DCR of the SiPM irradiated at 10^{12} neq/cm^2 only reaches the value before the irradiation around − 170 °C, with the annealing reducing the cooling requirement to about − 150°C. A similar 20°C reduction in cooling requirements can be observed for all other irradiation levels, except for the 10^{13} neq/cm^2. On the other hand, if cooling to only, for example, − 50°C was possible, irradiation to a maximum of 10^9 neq/cm^2 could be tolerated. This can also be seen with the same data rearranged to show the dependence on the fluence, as shown in Fig. 17. For example, the line indicating measurements at liquid nitrogen temperature reaches the DCR of the non-irradiated SiPM at room temperature and an overvoltage of 9 V (gray line) at a fluence of about 2×10^{12} neq/cm^2, which can be only slightly improved by the annealing as conducted in this work. The data in Fig. 16 can also be used to determine the cooling requirements for different tolerable DCR levels, shown in Fig. 18. The DCRs at which single photons could be resolved (Figs. 13 and 16) are about 1 MHz for all irradiation levels below 10^{13} neq/cm^2. For such DCR levels the results in Fig. 18 indicate liquid nitrogen cooling is necessary for irradiation levels above 10^{12} neq/cm^2, again with only small relaxation of requirements observable after the annealing.

A similar behavior of irradiated SiPMs with cooling was observed in [29], where it was reported that even when single photons could not be resolved after 10^9 neq/cm^2 at room temperature, single photons could be resolved again by cooling the same SiPM to 84 K (− 189°C). In addition, it was also shown that at 250°C the SiPM annealed to the extent where single photons could be resolved again after 10^9 neq/cm^2, even at room temperature. Whereas, in [30], it was also demonstrated that thermal annealing up to 175°C and cooling the SiPM down to 77 K (− 196°C) lead to the possibility of operating the SiPM with single photon discrimination after 10^{14} neq/cm^2. On the path of achieving the targeted SiPM radiation hardness alongside good timing performance, dedicated developments, together with radiation damage reduction and mitigation techniques, are needed. For example, if the noisiest SPADs of the SiPMs could be turned off, which is not the case for existing analog SiPMs as all the SPADs are connected in parallel, the DCR could be substantially decreased. Following this idea, in [37] it was shown that when only the three noisiest SPADs in irradiated 5 × 5 CMOS SPAD arrays are disabled, the DCR reduced from 51 to 18 kHz. Another strategy for improving SiPM radiation tolerance would be using smaller SPADs because their active area is less likely to be damaged [38]. However, this will also result in lower photon detection efficiency, which can be recovered by using optical enhancements like microlenses [39]. Even though these results look promising, more research is needed, and thermal annealing might be challenging to implement in the context of operational RICH detectors.

5 Conclusions

In this work, neutron-irradiated SiPMs with fluences from 10^9 neq/cm^2 up to 10^{13} neq/cm^2 were characterized at room temperature and at five equidistant stabilized temperatures down to the liquid nitrogen temperature. Besides, it was explored how the high-temperature annealing can improve their performance post-irradiation. It was observed that with increasing irradiation fluence, the I_{leak}, I_{dark}, and DCR worsened. Before the irradiation, an SPTR below 90 ps FWHM was measured, and it was observed to be unaffected by cooling down to the liquid nitrogen temperature. After the irradiation, the high DCR made single photon discrimination not possible at room temperature, even for the SiPM

irradiated at 10^9 neq/cm^2. Cooling was necessary to regain single photon discrimination, and with it, SPTR values below 100 ps FWHM. The results presented in this contribution indicate that cooling to liquid nitrogen temperature would be necessary for the examined SiPM technology to be useful in the planned RICH upgrades. As long as cooling applied was sufficient to discriminate single photons, SPTRs measured did not seem to be affected by the irradiation with values around 90 ps FWHM obtained for all the irradiation levels at SiPM overvoltage of 9 V except for the SiPM irradiated at 10^{13} neq/cm^2. The annealing of the SiPMs at 80°C for 24 h improved the performance only slightly, relaxing the cooling requirements for about 20°C as indicated by the measured DCRs. The presented experimental setup is planned to be used to characterize other SiPMs and test structures, and the results of this and future work will be used to guide the design of more radiation-resistant SiPMs and find the way to use SiPMs in highly irradiated environments at single photon level.

Acknowledgements We would like to thank Fondazione Bruno Kessler, especially A. Gola, S. Merzi, and M. Penna for providing the photodetector samples and related support. We would like to thank TRIGA nuclear reactor of Jožef Stefan Institute, especially A. Verdir, A. Jazbec, and S. Rupnik for the help with sample irradiation.

Funding The authors acknowledge the financial support from the AidaInnova project, EU Horizon 2020 RIA program, grant n.10100476, the Jennifer2, EU H2020 MSCA-RISE program, grant n.822070, and the financial support from the Slovenian Research and Innovation Agency (project J1-4358).

Data Availability Statement Data will be made available on reasonable request. [Authors' comment: The datasets generated during and/or analysed during the current study are available from the corresponding author on reasonable request.].

Code Availability Statement Code/software will be made available on reasonable request. [Authors' comment: The code/software generated during and/or analysed during the current study is available from the corresponding author on reasonable request.].

Funded by SCOAP[3].

References

1. S.A. Wotton et al., The LHCb RICH upgrade for high luminosity LHC era. Nucl. Instrum. Methods Phys. Res. A. **1058**, 168824 (2024). https://doi.org/10.1016/j.nima.2023.168824
2. K. Uno, Operation and performance of the Belle II Aerogel RICH detector. Nucl. Instrum. Methods Phys. Res. A. **1056**, 168635 (2023). https://doi.org/10.1016/j.nima.2023.168635
3. LHCb Collaboration, Framework TDR for the LHCb Upgrade II: opportunities in flavour physics, and beyond, in the HL-LHC era (2021). https://cds.cern.ch/record/2776420/
4. P. Buzhan et al., An advanced study of silicon photomultiplier. ICFA Instrum. Bull. **23**, 28–41 (2001)
5. B. Dolgoshein et al., Status report on silicon photomultiplier development and its applications. Nucl. Instrum. Methods Phys. Res. A. **563**, 368–376 (2006). https://doi.org/10.1016/j.nima.2006.02.193
6. F. Acerbi, S. Gundacker, Understanding and simulating SiPMs. Nucl. Instrum. Methods Phys. Res. A. **926**, 16–35 (2019). https://doi.org/10.1016/j.nima.2018.11.118
7. N. Aide et al., New PET technologies–embracing progress and pushing the limits. EJNMMI. **48**, 2711-2726 (2021). https://doi.org/10.1007/s00259-021-05390-4
8. S. Gundacker et al., On timing-optimized SiPMs for Cherenkov detection to boost low cost time-of-flight PET. Phys. Med. Biol. **68**, 165016 (2023). https://doi.org/10.1088/1361-6560/ace8ee
9. G. Razdevšek et al., Exploring the Potential of a Cherenkov TOF PET Scanner: A Simulation Study. IEEE Trans. Radiat. Plasma Med. Sci. **7**, 52–61 (2023). https://doi.org/10.1109/TRPMS.2022.3202138
10. R. Pestotnik et al., Module of silicon photomultipliers as a detector of individual Cherenkov photons. Nucl. Instrum. Methods Phys. Res. A. **639**, 99–102 (2011). https://doi.org/10.1016/j.nima.2010.09.122
11. A. Heering et al., Low temperature characteristics of SiPMs after very high neutron irradiation. Nucl. Instrum. Methods Phys. Res. A. **936**, 671–673 (2019). https://doi.org/10.1016/j.nima.2018.09.111
12. ALICE Collaboration, Letter of intent for ALICE 3: a next-generation heavy-ion experiment at the LHC (2022). https://doi.org/10.48550/arXiv.2211.02491
13. F. Simon, Silicon photomultipliers in particle and nuclear physics. Nucl. Instrum. Methods Phys. Res. A. **926**, 85–100 (2019). https://doi.org/10.1016/j.nima.2018.11.042
14. A. Morciano, et al., Signal-to-Noise Ratio in Pulsed Mode SiPMs for LiDAR Applications, in *IEEE International Conference on Integrated Circuit Design and Technology (ICICDT)*, Dresden (2021). https://doi.org/10.1109/ICICDT51558.2021.9626464
15. A. Ulyanov et al., Radiation damage study of SensL J-series silicon photomultipliers using 101.4 MeV protons. Nucl. Instrum. Methods Phys. Res. A. **976**, 164203 (2020). https://doi.org/10.1016/j.nima.2020.164203
16. L. Mitchell et al., Radiation damage assessment of SensL SiPMs. Nucl. Instrum. Methods Phys. Res. A. **988**, 164798 (2021). https://doi.org/10.1016/j.nima.2020.164798
17. A.R. Altamura et al., Radiation damage on SiPMs for space applications. Nucl. Instrum. Methods Phys. Res. A. **1045**, 167488 (2023). https://doi.org/10.1016/j.nima.2022.167488
18. S. Gundacker, A. Heering, The silicon photomultiplier: fundamentals and applications of a modern solid-state photon detector. Phys. Med. Biol. (2020). https://doi.org/10.1088/1361-6560/ab7b2d
19. S. Korpar et al., A module of silicon photo-multipliers for detection of Cherenkov radiation. Nucl. Instrum. Methods Phys. Res. A. **613**, 195–199 (2010). https://doi.org/10.1016/j.nima.2009.11.043

20. S. Korpar et al., Status and perspectives of solid state photon detectors. Nucl. Instrum. Methods Phys. Res. A. **639**, 88–93 (2011). https://doi.org/10.1016/j.nima.2010.10.154
21. M. Guarise et al., A newly observed phenomenon in the characterisation of SiPM at cryogenic temperature. JINST. **16**, T10006 (2011). https://doi.org/10.1088/1748-0221/16/10/T10006
22. D. Durini et al., Evaluation of the dark signal performance of different SiPM-technologies under irradiation with cold neutrons. Nucl. Instrum. Methods Phys. Res. A. **835**, 99–109 (2016). https://doi.org/10.1016/j.nima.2016.08.016
23. L. Ratti et al., Dark count rate degradation in CMOS SPADs exposed to X-rays and neutrons. IEEE Trans. Nucl. Sci. **66**, 567–574 (2019). https://doi.org/10.1109/TNS.2019.2893233
24. F. Acerbi et al., Cryogenic Characterization of FBK HD Near-UV Sensitive SiPMs. IEEE Trans. Electron Devices **64**, 521–526 (2017). https://doi.org/10.1109/TED.2016.2641586
25. C. Piemonte, A. Gola, Overview on the main parameters and technology of modern silicon photomultipliers. Nucl. Instrum. Methods Phys. Res. A. **926**, 2–15 (2019). https://doi.org/10.1016/j.nima.2018.11.119
26. B. Chana et al., Rapid characterization of silicon photomultipliers for noble liquid experiments. JINST. **18**, C03004 (2023). https://doi.org/10.1088/1748-0221/18/03/C03004
27. A.R. Altamura et al., Characterization of Silicon Photomultipliers after proton irradiation up to 10^{14} neq/cm^2. Nucl. Instrum. Methods Phys. Res. A. **1040**, 167284 (2022). https://doi.org/10.1016/j.nima.2022.167284
28. E. Garutti, Yu. Musienko, Radiation damage of SiPMs. Nucl. Instrum. Methods Phys. Res. A. **926**, 69–84 (2019). https://doi.org/10.1016/j.nima.2018.10.191
29. T. Tsang et al., Neutron radiation damage and recovery studies of SiPMs. JINST. **11**, P12002 (2016). https://doi.org/10.1088/1748-0221/11/12/P12002
30. M. Calvi et al., Single-photon detection with SiPMs irradiated up to 10^{14} neq/cm^2 1-MeV-equivalent neutron fluence. Nucl. Instrum. Methods Phys. Res. A. **922**, 243–249 (2019). https://doi.org/10.1016/j.nima.2019.01.013
31. A. Gola et al., NUV-sensitive silicon photomultiplier technologies developed at Fondazione Bruno Kessler. Sensors. **19**, 308 (2019). https://doi.org/10.3390/s19020308
32. NEC Bipolar Analog Integrated Circuit μPC2710TB Data Sheet, NEC Corporation (2001)
33. H. Friederich et al., A scalable DAQ system based on the DRS4 waveform digitizing chip. IEEE Trans. Nucl. Sci. **58**, 1652–1656 (2011). https://doi.org/10.1109/TNS.2011.2159623
34. R. Brun, F. Rademakers, ROOT–an object-oriented data analysis framework. Nucl. Instrum. Methods Phys. Res. A. **389**, 81-86 (1997). https://doi.org/10.1016/S0168-9002(97)00048-X
35. L. Snoj et al., Radiation hardness studies and detector characterisation at the JSI TRIGA reactor. EPJ Web Conf. **225**, 04031 (2020). https://doi.org/10.1051/epjconf/202022504031
36. A. Prêle et al., SiPM cryogenic operation down to 77 K, in *10th International Workshop On Low Temperature Electronics (WOLTE10)*, Paris (2013)
37. M. Campajola et al., Comparison of proton and electron radiation effects on dark count rate in a CMOS SPAD sensor. Proc. SPIE (2020). https://doi.org/10.1117/12.2559507
38. M.-L. Wu et al., Radiation hardness study of single-photon avalanche diode for space and high energy physics applications. Sensors **22**, 2919 (2022). https://doi.org/10.3390/s22082919
39. C. Bruschini et al., Challenges and prospects for multi-chip microlens imprints on front-side illuminated SPAD imagers. Opt. Express **31**, 21935–21953 (2023). https://doi.org/10.1364/OE.488177